

Disk reflection and a possible disk wind during a soft X-ray state in the neutron star low-mass X-ray binary 1RXS J180408.9–342058

N. Degenaar^{1,2*}, D. Altamirano³, M. Parker¹, J.C.A. Miller-Jones⁴, J.M. Miller⁵, C.O. Heinke⁶, R. Wijnands², R. Ludlam⁵, A. Parikh², J.W.T. Hessels^{2,7}, N. Gusinskaia², A.T. Deller⁷ and A.C. Fabian¹

¹*Institute of Astronomy, University of Cambridge, Madingley Road, Cambridge CB3 0HA, UK*

²*Anton Pannekoek Institute for Astronomy, University of Amsterdam, Science Park 904, 1098 XH, Amsterdam, the Netherlands*

³*School of Physics and Astronomy, University of Southampton, Southampton, Hampshire, SO171BJ, UK*

⁴*International Centre for Radio Astronomy Research, Curtin University, GPO Box U1987, Perth, WA 6845, Australia*

⁵*Department of Astronomy, University of Michigan, 1085 South University Avenue, Ann Arbor, MI 48109, USA*

⁶*Department of Physics, University of Alberta, 4-183 CCIS, Edmonton, AB T6G 2E1, Canada*

⁷*ASTRON, the Netherlands Institute for Radio Astronomy, Postbus 2, 7990 AA, Dwingeloo, The Netherlands*

Accepted to MNRAS Main Journal

ABSTRACT

1RXS J180408.9–342058 is a transient neutron star low-mass X-ray binary that exhibited a bright accretion outburst in 2015. We present *NuSTAR*, *Swift*, and *Chandra* observations obtained around the peak brightness of this outburst. The source was in a soft X-ray spectral state and displayed an X-ray luminosity of $L_X \simeq (2-3) \times 10^{37} (D/5.8 \text{ kpc})^2 \text{ erg s}^{-1}$ (0.5–10 keV). The *NuSTAR* data reveal a broad Fe-K emission line that we model as relativistically broadened reflection to constrain the accretion geometry. We found that the accretion disk is viewed at an inclination of $i \simeq 27^\circ-35^\circ$ and extended close to the neutron star, down to $R_{\text{in}} \simeq 5-7.5$ gravitational radii ($\simeq 11-17 \text{ km}$). This inner disk radius suggests that the neutron star magnetic field strength is $B \lesssim 2 \times 10^8 \text{ G}$. We find a narrow absorption line in the *Chandra*/HEG data at an energy of $\simeq 7.64 \text{ keV}$ with a significance of $\simeq 4.8\sigma$. This feature could correspond to blue-shifted Fe XXVI and arise from an accretion disk wind, which would imply an outflow velocity of $v_{\text{out}} \simeq 0.086c$ ($\simeq 25\,800 \text{ km s}^{-1}$). However, this would be extreme for an X-ray binary and it is unclear if a disk wind should be visible at the low inclination angle that we infer from our reflection analysis. Finally, we discuss how the X-ray and optical properties of 1RXS J180408.9–342058 are consistent with a relatively small ($P_{\text{orb}} \lesssim 3 \text{ hr}$) binary orbit.

Key words: accretion: accretion disks – stars: individual (1RXS J180408.9–342058) – stars: neutron – stars: winds, outflows – X-rays: binaries

1 INTRODUCTION

Low-mass X-ray binaries (LMXBs) consist of a neutron star or a black hole plus a companion star that is less massive than the compact primary. The companion typically overflows its Roche-lobe, thereby feeding gas to an accretion disk that surrounds the neutron star or black hole. In transient systems, outbursts of active accretion are interleaved with long periods of quiescence when the accretion rate onto the compact primary is strongly reduced. LMXBs are excellent laboratories to investigate how accretion proceeds under the influence of strong gravity over a wide range of accretion rates.

X-ray spectroscopy is a powerful tool to study accretion processes in LMXBs; both the X-ray continuum spectral shape and discrete emission/absorption features give insight into the accre-

tion geometry. Broadly speaking, two main X-ray spectral states can be distinguished during the active phases of LMXBs (see e.g., Homan & Belloni 2005; Remillard & McClintock 2006, for a detailed overview). During a “soft state”, thermal emission from the accretion disk is prominently detected in the X-ray spectrum. However, during a “hard state”, the disk emission is much weaker and a strong non-thermal, hard X-ray emission component is seen that likely arises from a hot plasma in the inner accretion flow.

Hard X-rays can illuminate the accretion disk and produce a reflection spectrum of emission lines, the most prominent being Fe-K at 6.4–6.97 keV (e.g., George & Fabian 1991; Matt et al. 1991). The shape of such lines depends on the chemical abundances and ionization state of the accretion disk, but also on its inner radial extent since both relativistic and dynamical effects act to broaden reflected emission lines. Disk reflection studies suggest that in some neutron star LMXBs the stellar magnetic field is strong

* e-mail: degenaar@ast.cam.ac.uk

enough to truncate the inner accretion disk (Degenaar et al. 2014a; Pintore et al. 2016; King et al. 2016), whereas in others it can extend all the way down to the innermost stable circular orbit (ISCO) or the neutron star surface (e.g., Bhattacharyya & Strohmayer 2007; D’Ai et al. 2009; Papitto et al. 2009; Cackett et al. 2010; Miller et al. 2013; Degenaar et al. 2015a; Di Salvo et al. 2015).

High-resolution X-ray spectroscopy of LMXBs can reveal narrow, blue-shifted absorption features arising from a highly ionized wind that is blown off the accretion disk (e.g., Brandt & Schulz 2000; Ueda et al. 2004; Miller et al. 2006b, 2016; Díaz Trigo et al. 2007; Bozzo et al. 2016). These winds are preferentially detected during soft X-ray spectral states (e.g., Miller et al. 2006a, 2008; Neilsen & Lee 2009; Ponti et al. 2012). Typical outflow velocities are $\simeq 400\text{--}3000\text{ km s}^{-1}$ ($\simeq 0.001\text{--}0.01c$) and the properties are very similar in black hole and neutron star LMXBs (e.g., Díaz Trigo & Boirin 2016). Powerful disk winds may carry away a significant amount of mass, similar to or even exceeding the amount of mass that is accreted (e.g., Lee et al. 2002; Neilsen et al. 2011; King et al. 2012, 2015; Ponti et al. 2012; Degenaar et al. 2014a). Winds are therefore important in considering the energy budget of the accretion process, and may also lead to instabilities in the accretion flow (e.g., Begelman & McKee 1983; Shields et al. 1986).

1.1 1RXS J180408.9–342058 (RXS J1804)

1RXS J180408.9–342058, hereafter referred to as RXS J1804, was detected as a faint X-ray source with *ROSAT* in 1990 (Voges et al. 1999). It remained unclassified until 2012, when *Integral* detected a thermonuclear X-ray burst that identified RXS J1804 as an accreting neutron star in, most likely, an LMXB. Assuming that the peak luminosity of the X-ray burst did not exceed the empirically-determined Eddington limit ($L_{\text{Edd}} = 3.8 \times 10^{38}\text{ erg s}^{-1}$; Kuulkers et al. 2003), places the source at a distance of $D \lesssim 5.8\text{ kpc}$ (Chenevez et al. 2012).

No persistent emission could be detected with *Integral* when the X-ray burst was seen in 2012, implying an accretion luminosity of $L_X \lesssim 4 \times 10^{35}\text{ erg s}^{-1}$ at the time (3–10 keV). Indeed, follow-up *Swift* observations detected the source at $L_X \simeq 10^{33} - 10^{34}\text{ erg s}^{-1}$ (0.5–10 keV), suggesting that it had exhibited a faint accretion outburst that was missed by all-sky monitors (Chenevez et al. 2012; Kaur & Heinke 2012).

In 2015 January, an outburst from RXS J1804 was seen by *Swift*/BAT and *MAXI* monitoring observations (Krimm et al. 2015b; Negoro et al. 2015). Figure 1 shows the publicly available *MAXI* (2–20 keV; Matsuoka et al. 2009)¹ and *Swift*/BAT (15–50 keV; Krimm et al. 2013)² daily monitoring light curves of this outburst. The source remained at relatively constant flux in a hard X-ray spectral state (Ludlam et al. 2016) for $\simeq 2$ months, during which radio emission from a jet was detected (Deller et al. 2015). Around April 3, however, the source transitioned to a soft X-ray spectral state (Degenaar et al. 2015b, dotted line in Figure 1). The activity ceased $\simeq 2$ months later, i.e., the total outburst duration was $\simeq 4.5$ months (see Figure 1).

In this work we report on X-ray spectral observations of RXS J1804 obtained with *NuSTAR* (Harrison et al. 2013), *Swift* (Gehrels et al. 2004), and *Chandra* (Weisskopf et al. 2000). These data were taken during the soft X-ray spectral state near the peak brightness of the 2015 outburst (see Table 1 and Figure 1).

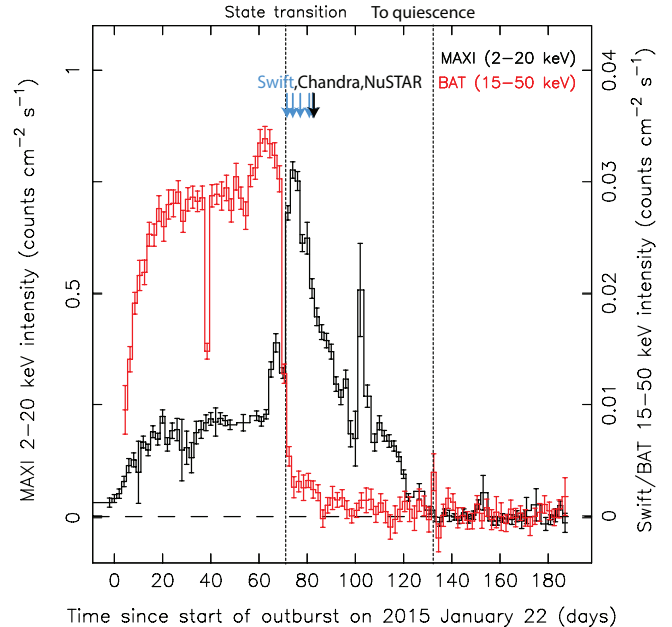


Figure 1. Combined *Swift*/BAT (red, 15–50 keV) and *MAXI* (black, 2–20 keV) X-ray light curves of the 2015 outburst of RXS J1804 (2-day bins). The hard to soft state transition and the estimated return to quiescence are indicated by the vertical dotted lines. Times of the *Chandra*, *NuSTAR* and *Swift*/XRT observations discussed in this work are indicated by the arrows.

2 OBSERVATIONS AND DATA ANALYSIS

2.1 *NuSTAR*

RXS J1804 was observed with *NuSTAR* between 12:11 UT on 2015 April 14 and 00:51 UT on April 15 (Obs ID 90101003002), i.e. $\simeq 9$ d after the transition to the soft spectral state (see Figure 1). *NuSTAR* consists of two co-aligned grazing incidence hard X-ray imaging telescopes, the focal plane mirror (FPM) A and B, which provide sensitivity in an energy range of 3–79 keV. As such, it is a particularly powerful instrument to study disk reflection spectra.

Standard screening and processing with NUSTARDAS, incorporated in HEASOFT (v. 6.17), resulted in $\simeq 20$ ks of on-target exposure time per mirror. We employed NUPRODUCTS to create light curves and spectra for the FPMA and FPMB. A circular region with a radius of $60''$ was used to extract source events and a void region of the same size, placed on the same CCD, was used to extract background events. The summed FPMA/B count rate varied between $\simeq 180\text{--}230\text{ c s}^{-1}$ during the observation (3–79 keV).

All spectral data were grouped into bins with a minimum of 20 photons using GRPPHA. We found that RXS J1804 was detected significantly above the background up to $\simeq 35$ keV, so we restricted our spectral fits of the *NuSTAR* data to an energy range of 3–35 keV. The separate spectra obtained for the two mirrors were fitted simultaneously with all parameters tied, but with a constant factor varying between them to account for calibration uncertainties.

2.2 *Chandra*

We observed RXS J1804 with *Chandra* on 2015 April 14 between 14:55 and 23:54 UT (Obs ID 17649) for $\simeq 30$ ks. The High Energy Transmission Grating (HETG; Canizares et al. 2000) was used to disperse the incoming light onto the ACIS-S array, enabling high X-ray spectroscopy to search for narrow spectral features. We fo-

¹ <http://maxi.riken.jp/top/index.php?cid=1&jname=J1804-343>

² <http://swift.gsfc.nasa.gov/results/transients/weak/1RXSJ180408.9-342058/>

Table 1. Log of the (soft state) observations considered in this work.

Instrument	ObsID	Start time (MJD)	Exposure time (ks)
<i>Swift</i> (XRT/WT)	32436029	57115.83	1.1
<i>Swift</i> (XRT/WT)	32436030	57118.18	1.0
<i>Swift</i> (XRT/WT)	32436031	57121.17	1.0
<i>Swift</i> (XRT/WT)	32436032	57124.16	1.0
<i>NuSTAR</i>	90101003002	57126.51	20.2
<i>Swift</i> (XRT/WT)	81451001	57126.54	1.0
<i>Chandra</i> (HETG)	17649	57126.62	30.0

cus on the data from the High Energy Grating (HEG) arm, since it has better energy resolution and extends to higher energies than the Medium Energy Grating (MEG), and is therefore best suited for studying highly ionized disk winds. The ACIS CCD was operated in continuous clocking (CC) mode to mitigate the effects of pile-up. Furthermore, a 100-column “gray window” was placed over the aimpoint to ensure that only one in every ten zeroth-order event was read out, to limit telemetry saturation and loss of frames.

We reduced the *Chandra* data using CIAO (v. 4.8). We followed the standard steps for CC-mode data reduction³, except that we ran TG_CREATE_MASK with a width factor of 15, rather than the default 35. We used this narrower extraction region in an attempt to reduce noise. RXS J1804 was detected at a HEG count rate of $\simeq 50\text{--}60 \text{ c s}^{-1}$ (0.8–10 keV). We did not find significant differences between the spectra of the plus and minus grating orders such as e.g., discussed in Chiang et al. (2016). We therefore combined the first-order positive and negative grating data using COMBINE_GRATING_SPECTRA. To avoid instrumental artifacts present in CC mode data of bright sources, we restricted the *Chandra*/HEG spectral fits to 2–9 keV (see e.g., Cackett et al. 2009b; Miller et al. 2011, 2012; Chiang et al. 2016).

2.3 *Swift*

To follow the global X-ray spectral and flux evolution, the outburst of RXS J1804 was monitored using many short ($\simeq 1\text{--}2$ ks) pointed *Swift* observations, providing 0.3–10 keV coverage with the XRT (e.g., Degenaar et al. 2015b; Deller et al. 2015; Krimm et al. 2015a; Baglio et al. 2016). Here, we aim to characterize the tentative high-energy absorption features reported by Degenaar et al. (2015b). We therefore focus on five soft-state observations obtained around the peak of the outburst between 2015 April 3–14 (Table 1). Observation 81451001 was performed simultaneously with our *NuSTAR* observation, and we used this data for broad-band spectral fitting.

The *Swift* data were analyzed using standard tools incorporated in HEASOFT (v. 6.17). All observations considered in this work were obtained in the windowed timing (WT) mode. We used XSELECT to extract source events from a box-shaped region with a length of $70''$. Background events were obtained from the outer regions of the CCD, avoiding the inner $280''$ around the source. In all observations considered here, the XRT count rate was $>100 \text{ c s}^{-1}$ and hence sufficiently high to cause pile-up. Following the recommended procedure, we therefore excised as many inner pixels as needed for the spectrum to remain unchanged after removing more pixels (e.g., Romano et al. 2006). This resulted in the exclusion of the inner $2''$ for all five XRT observations.

Exposure maps were used to create ancillary response files

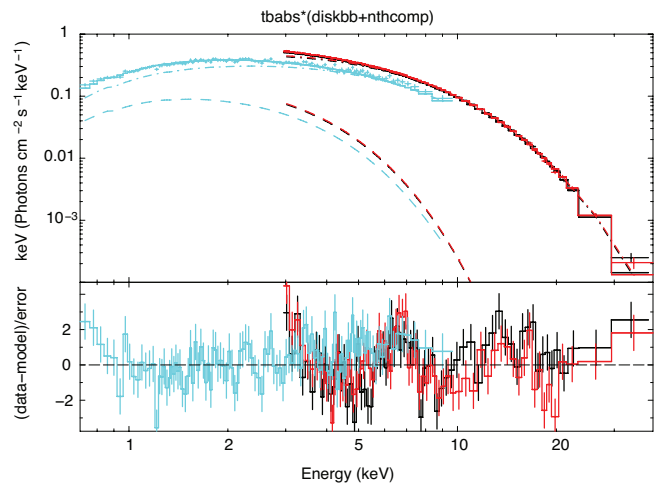


Figure 2. *NuSTAR* (FPMA in black, FPMB in red) and *Swift*/XRT (cyan) unfolded spectra (rebinned for visual clarity). Solid curves represent a fit to a continuum model consisting of a disk black body (dashed curves), and Comptonized emission (dashed-dotted curves). The bottom panel shows the residuals in sigmas, revealing un-modeled structure near 6–7 keV that likely also causes deviations from the model at lower and higher energies.

with XRTMKARF, to account for hot pixels and bad columns on the CCD. The latest response matrix file was sourced from the calibration data base (v. 15). Spectra were grouped to contain a minimum of 20 photons per bin and spectral fits were performed in an energy range of 0.7–10 keV to avoid instrumental artifacts present for bright sources observed in WT mode.⁴

2.4 Spectral analysis and assumed quantities

All spectral fits reported in this work were performed within XSPEC (v. 12.9; Arnaud 1996). For each fit we included the TBABS model to account for interstellar absorption along the line of sight. Abundances were set to WILM (Wilms et al. 2000), and cross-sections to VERN (Verner et al. 1996). The total model 0.7–35 keV flux and error were determined with the CFLUX convolution model. When fitting spectral data from different instruments together, we used a constant multiplication factor (C) to allow for cross-calibration uncertainties. Throughout this work, we assume a source distance of $D=5.8$ kpc, an Eddington limit of $L_{\text{Edd}}=3.8 \times 10^{38} \text{ erg s}^{-1}$ (Kuulkers et al. 2003), and a neutron star mass of $M=1.5 M_{\odot}$. Errors are given at 1σ confidence level.

3 RESULTS

3.1 Broad-band X-ray spectrum in the soft state

The *NuSTAR* observation of RXS J1804 was carried out simultaneously with the *Chandra*/HEG observation and the *Swift*/XRT observation with ID 81451001 (see Table 1). Since the *Swift* data are more reliable to lower energies than our *Chandra* data (see Section 2), we choose to use the *Swift* observation together with the *NuSTAR* data to perform broad-band spectral fits.

We fitted the 0.7–35 keV *NuSTAR*/*Swift* continuum to a

³ <http://cxc.harvard.edu/ciao/why/ccmode.html>

⁴ See http://www.swift.ac.uk/analysis/xrt/digest_cal.php.

model consisting of thermal Comptonization and a soft emission component. For the latter we used DISKBB, and for the former we used NTHCOMP with seed photons provided by a disk black body (Zdziarski et al. 1996; Życki et al. 1999). The NTHCOMP model has a power-law component with an index Γ , a low-energy cutoff set by the seed photon temperature (kT_s) and a high energy roll-over determined by the electron temperature (kT_e). This two-component model often provides a good description of the broad-band continuum of neutron star LMXBs in their soft spectral states (e.g., Barret & Olive 2002; Piraino et al. 2007; Di Salvo et al. 2015; King et al. 2016). It may be physically interpreted as direct emission from the accretion disk and Comptonized emission from either a hot flow or a boundary layer where the disk runs into the neutron star surface, with the seed photons provided by the disk and/or surface of the neutron star (e.g., Barret et al. 2000; Di Salvo et al. 2000).

Our continuum model can describe the 0.7–35 keV *NuSTAR*/*Swift* spectral data reasonably well ($\chi^2_\nu=1.05$ for 1495 dof; Figure 2). We obtain a hydrogen column density of $N_{\text{H}}=(3.3 \pm 0.2) \times 10^{21} \text{ cm}^{-2}$ and an inner disk temperature of $kT_{\text{in}}=0.89 \pm 0.07 \text{ keV}$. For the NTHCOMP component we obtain $\Gamma=2.6 \pm 0.1$, $kT_s=1.51 \pm 0.13 \text{ keV}$, and $kT_e=2.72 \pm 0.07 \text{ keV}$. The 0.7–35 keV unabsorbed flux inferred from this fit is $F_{0.7-35} \simeq 4.7 \times 10^{-9} \text{ erg cm}^{-2} \text{ s}^{-1}$, which translates into a luminosity of $L_{0.7-35} \simeq 1.9 \times 10^{37} (D/5.8 \text{ kpc})^2 \text{ erg s}^{-1}$. The disk contribution to the total 0.7–35 keV flux is $\simeq 35\%$. We note that a continuum consisting of a black body, a (broken) power law and a disk black body is also frequently used for soft state spectra of neutron star LMXBs (e.g., Lin et al. 2007; Cackett et al. 2010; Miller et al. 2013). Such a model fits our data less well ($\chi^2_\nu=1.06$ for 1495 dof).

Figure 2 shows that our continuum description leaves residuals near 6–7 keV. These are likely due to a broad Fe-K emission line that arises from disk reflection, as was also seen during the hard state early on in the 2015 outburst of RXS J1804 (Ludlam et al. 2016).⁵ We therefore continued our spectral analysis by including physical reflection models.

3.2 Reflection spectrum

For neutron star LMXBs in their soft states, the X-ray spectrum above $\simeq 5 \text{ keV}$ is typically modeled as either a hot ($\simeq 2$ – 3 keV) black body or thermal Comptonization. This emission component provides most of the hard X-ray flux that illuminates the accretion disk and produces the reflection spectrum (e.g., Cackett et al. 2010). We therefore used a modified version of REFLECTIONX (Ross & Fabian 2005) that assumes a black body input spectrum.⁶ Although our broad-band fits prefer a Comptonized model over a black body to describe the spectrum above $\simeq 5 \text{ keV}$ (see Section 3.1), we found that this reflection model works very well for our data. This is presumably because the Comptonized emission can be approximated by a hot black body and because the Fe-K line in our data is relatively weak, as is typically the case in soft spectral states. The fit parameters of the REFLECTIONX model are the ionization parameter ξ , the iron abundance A_{Fe} (with respect to

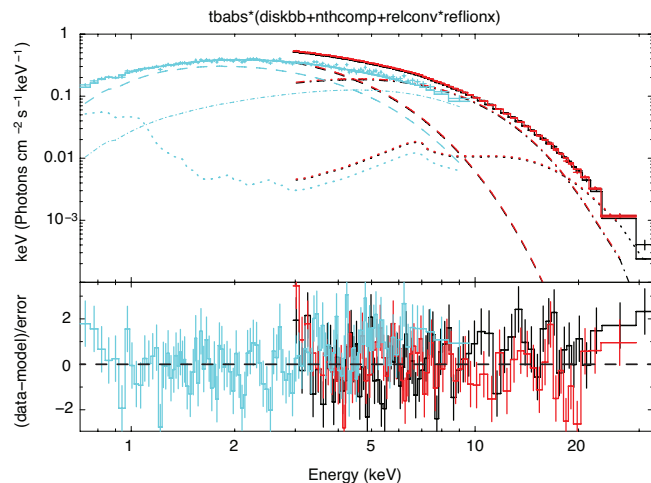


Figure 3. *NuSTAR* (FPMA in black, FPMB in red) and *Swift*/XRT (cyan) unfolded spectra fitted with a model consisting of a disk black body (dashed curves), Comptonized emission (dashed-dotted curves), and relativistically blurred reflection (dotted curves). The bottom panel shows the residuals in sigmas. The spectral data were rebinned for visual clarity.

Solar), the temperature of the ionizing black body flux (kT_{ref}), and a normalization (N_{ref}).

To account for broadening due to relativistic effects in the vicinity of the neutron star, we use the blurring kernel RELCONV with an unbroken emissivity profile of the form $\epsilon \propto r^{-q}$. The fit parameters of the RELCONV model are the emissivity index q , the inner and outer disk radius R_{in} and R_{out} (expressed in R_{ISCO}), the disk inclination (i), and the dimensionless spin parameter a . We fixed $q=3$ (appropriate for neutron star LMXBs, see e.g., Cackett et al. 2010), because this parameter was poorly constrained when left free to vary. We also fixed $R_{\text{out}}=500 R_{\text{ISCO}}$, since this emissivity profile drops off steeply with increasing radius so that the reflection fits are not sensitive to the outer disc radius.

The spin period of RXS J1804 is unknown, but neutron stars rotate slowly enough for the spin to have little effect on the metric. For neutron stars, the dimensionless spin parameter can be approximated as $a \simeq 0.47/P_{\text{ms}}$, where P_{ms} is the spin period in ms (Braje et al. 2000). The fastest known neutron stars spin at $\simeq 1.5 \text{ ms}$ (e.g., Galloway et al. 2008), i.e., $a \simeq 0.3$. Using equation 3 from Miller et al. (1998), the innermost stable circular orbit (ISCO) is then located at $R_{\text{isco}}=5.05 R_g (\simeq 11.2 \text{ km})$, where $R_g=GM/c^2$ is the gravitational radius (with G the gravitational constant and M the neutron star mass, which we assume to be $1.5 M_\odot$). This is thus only a small shift compared to the Schwarzschild metric ($a=0$) for which $R_{\text{isco}}=6 R_g (\simeq 13.3 \text{ km})$.

Including relativistic reflection significantly improves our spectral fits ($\chi^2_\nu=0.98$ for 1489 dof). The best fit parameters for the continuum and reflection spectrum are listed in Table 2. Our fits suggest that the inner disk was located close to the neutron star, at $R_{\text{in}}=1-1.5 R_{\text{ISCO}} (\simeq 5-7.5 R_g \text{ or } \simeq 11-17 \text{ km})$, and is viewed at an inclination of $i=29^\circ-35^\circ$. The obtained Fe abundance is consistent with Solar composition ($A_{\text{Fe}}=1.2 \pm 0.4$) and the disk appears to be mildly ionized ($\log \xi \simeq 2.1$). We note that fits performed with $a=0$ yielded similar results as for $a=0.3$, as expected. Figure 3 shows our fit results with relativistically blurred reflection included.

The normalization of the DISKBB spectral component can formally also be used to probe the inner radial extent of the accretion disk, as it is defined as $N_{\text{diskbb}}=(R_{\text{in,diskbb}}/D_{10})^2 \cos i$ (with

⁵ An alternative interpretation of these broad features as a mixture of number of narrower emission lines (see e.g., Ng et al. 2010, for a discussion) can be ruled out for at least some LMXBs (e.g., Chiang et al. 2016).

⁶ Available at http://www.xray.ast.cam.ac.uk/~mlparker/reflionx_models/reflionx_alking_mod.

Table 2. Results from fitting *NuSTAR* and *Swift* spectral data to a model CONSTANT*TBABS*(DISKBB+NTHCOMP+RELCONV*REFLIONX).

Parameter (unit)	value
C (FMPB)	1.034 ± 0.002
C (XRT)	0.682 ± 0.005
N_H ($\times 10^{21}$ cm $^{-2}$)	4.8 ± 0.2
kT_{in} (keV)	1.15 ± 0.02
N_{diskbb} (km/10 kpc) 2 cos i)	$91.9^{+5.8}_{-9.1}$
kT_s (keV)	1.27 ± 0.45
kT_e (keV)	1.87 ± 0.04
Γ	1.3 ± 0.2
N_{nthcomp} ($\times 10^{-2}$)	9.1 ± 0.1
i ($^\circ$)	32.2 ± 3.0
R_{in} ($\times R_{\text{ISCO}}$)	$1.0^{+0.5}$
ξ (erg cm s $^{-1}$)	119.4 ± 6.8
A_{Fe} (\times Solar)	1.2 ± 0.4
kT_{refl} (keV)	2.96 ± 0.07
N_{refl}	1.8 ± 0.5
$F_{0.7-35}$ ($\times 10^{-9}$ erg cm $^{-2}$ s $^{-1}$)	4.80 ± 0.01
$L_{0.7-35}$ ($\times 10^{37}$ ($D/5.8$ kpc) 2 erg s $^{-1}$)	1.93 ± 0.01
χ^2_{ν} (dof)	0.98 (1489)

Note. – We fixed $a=0.3$, $q=3$ and $R_{\text{out}}=500 R_{\text{ISCO}}$ for RELCONV and assumed disk black body seed photons for NTHCOMP. The constant multiplication factor was fixed to $C=1$ for the *NuSTAR* FMPA data, and left free for the other instruments. $F_{0.7-35}$ gives the total unabsorbed model flux in the 0.7–35 keV band, and $L_{0.7-35}$ is the corresponding luminosity for $D=5.8$ kpc. Quoted errors reflect 1σ confidence levels.

$R_{\text{in,diskbb}}$ in km and D_{10} the distance in units of 10 kpc). However, several (not well-determined) correction factors need to be taken into account to infer inner-disk radii from DISKBB fits, e.g., for inner boundary assumptions (Gierliński et al. 1999) and spectral hardening (Merloni et al. 2000), which may add up to a factor of $\simeq 1.7$ (e.g., Kubota et al. 2001; Reynolds & Miller 2013). Furthermore, uncertainties in the absolute flux calibration of the instrument or the spectral model (e.g., the column density or inclination) directly affect the inner disk radius inferred from the DISKBB model.

Bearing these caveats in mind, we note that the measured disk normalization of our best fit (Table 2) translates into an inner disk radius of $R_{\text{in,diskbb}}=6.0 \pm 0.4$ km for an inclination of $i=29^\circ-35^\circ$ (and $D_{10}=0.58$), without applying any corrections. Taking into account that the true inner disk radius may be a factor $\simeq 1.7$ higher yields $R_{\text{in,diskbb}}\simeq 9.5-11$ km. This is consistent with the location of the inner disk inferred from our reflection fits ($R_{\text{in}}\simeq 11-17$ km).

3.3 High-energy absorption features

3.3.1 *Swift*/XRT soft-state spectra

Degenaar et al. (2015b) reported hints of narrow absorption features near 7–8 keV in *Swift*/XRT spectra obtained after the transition to the soft state. This is illustrated by the top panel in Figure 4, which shows the high-energy residuals after fitting the first

soft-state observation (ID 32436029) to a simple two-component continuum consisting of a black body and a disk black body.⁷

Adding a Gaussian (GAUSS) with a central energy constrained to 7–8.5 keV suggests that an absorption feature may be present at $E_l=(7.26 \pm 0.06)$ keV. The width of the line appears unresolved and was therefore fixed to $\sigma_l = 10^{-4}$ keV. Dividing the normalization of the line by its 1σ error suggests that the feature is $\simeq 3.2\sigma$ significant. We measure an equivalent width of $EW\simeq 82$ eV. As can be seen in the bottom panel of Figure 4, a similar feature is seen at roughly the same energy in an observation performed 5 days later (ID 32436031; see Table 1). Adding a Gaussian to the continuum fit for this observation returns a central line energy of $E_l=(7.18 \pm 0.05)$ keV, a significance of $\simeq 3.6\sigma$, and $EW\simeq 89$ eV. We note that considering the number of trials by counting the observations searched (5) and the number of resolution elements in the search area (7), the significance of the features reduces to $\simeq 2\sigma$ and $\simeq 3\sigma$ for observation 32436029 and 32436031, respectively. The line parameters and the continuum fluxes are listed in Table 3.

Since the line energies obtained from the two spectra have overlapping 1σ errors and the measured continuum fluxes were similar (see Table 3), we also fitted them together with the line parameters tied. This yielded $E_l = (7.24 \pm 0.02)$ keV and a significance of $\simeq 4.8\sigma$ ($\simeq 4\sigma$ after accounting for trials). The 0.5–10 keV luminosity during these two observations was $L_{0.5-10}\simeq (2.9-3.2) \times 10^{37}$ ($D/5.8$ kpc) 2 erg s $^{-1}$. There are no features of similar significance detected in the other three soft-state XRT observations.

3.3.2 Narrow absorption lines in the *Chandra*/HEG data

The *Chandra*/HEG data provide superior spectral resolution and are therefore more suitable to detect and characterize narrow absorption features. Our observation was performed $\simeq 9$ days after the transition to the soft state, and $\simeq 5-9$ days after the possible absorption line detections in the *Swift*/XRT data (see Table 1).

To have the best constraints on the continuum, we fitted the *Chandra* data together with our simultaneous *NuSTAR* and *Swift* observations to our model described in Section 3.2 (Table 2). This fit leaves negative residuals in the HEG data near $\simeq 7$ and $\simeq 8$ keV, as shown in Figure 5. We characterized these two absorption features by adding simple Gaussian lines to our spectral fits and estimated their significance by dividing the normalization of the lines by the 1σ errors. The line normalization was set to zero for the *NuSTAR* and *Swift* data because the energy resolution of these instruments renders them insensitive to the very narrow features that we find in the *Chandra* data (see below). The width of the lines was unconstrained and therefore fixed at $\sigma_l=10^{-4}$ keV. We also noted an absorption feature in the HEG data near 5.5 keV, but it was not present in the MEG data and hence likely spurious.

The line properties and continuum flux are listed in Table 3. For the first line we obtain a central energy of $E_l=7.64 \pm 0.01$ keV, a significance of $\simeq 5.8\sigma$, and an equivalent width of $EW\simeq 18$ eV. A second absorption feature is found at $E_l=8.26 \pm 0.07$ keV, with a significance of $\simeq 3.6\sigma$ and $EW\simeq 23$ eV. When accounting for the number of trials, the significance decreases to $\simeq 4.8\sigma$ and $\simeq 2\sigma$, respectively. Both features are also seen in the separate plus and minus order spectra, albeit at lower significance. There are no chip

⁷ When using DISKBB+NTHCOMP, several of the parameters were not well-constrained, presumably due to the narrow energy range and limited sensitivity of the XRT data. We therefore used this simpler continuum model for the *Swift* data, which provided a good description.

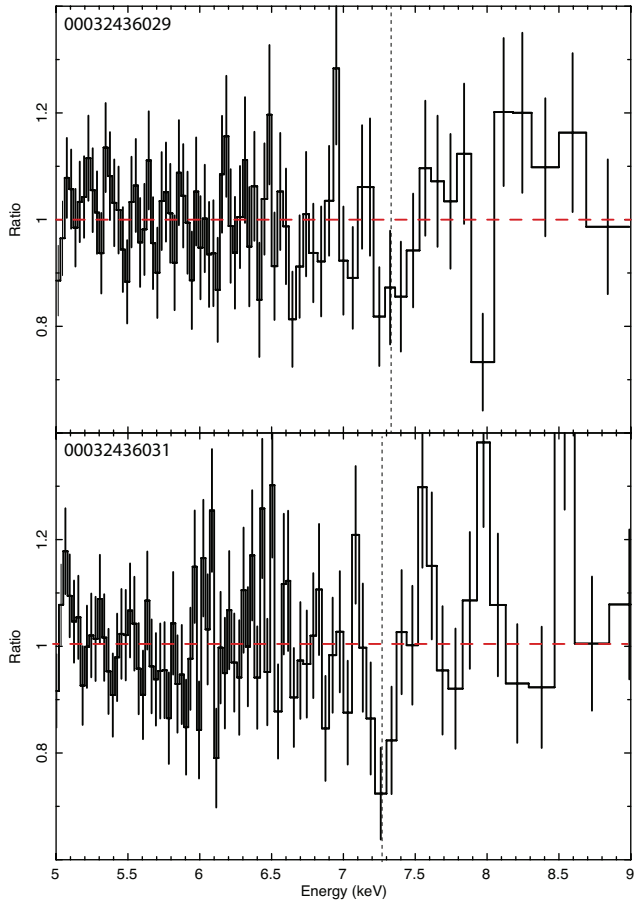


Figure 4. *Swift*/XRT data to model ratio in the 5–9 keV range for a simple 2-component continuum consisting of a black body and a disk black body. Negative residuals are present near $\simeq 7.2$ keV (dotted vertical lines), which were not seen during the other three soft-state observations.

Table 3. Narrow absorption lines in *Chandra* and *Swift* spectral data.

Instrument	ObsID	E_1 (keV)	$F_{0.5-10}$ ($\text{erg cm}^{-2} \text{s}^{-1}$)
<i>Swift</i> /XRT	32436029	7.26 ± 0.06	7.2×10^{-9}
<i>Swift</i> /XRT	32436031	7.18 ± 0.05	7.9×10^{-9}
<i>Swift</i> /XRT	32436029+31	7.24 ± 0.04	
<i>Chandra</i> /HEG	17649	7.64 ± 0.01	5.2×10^{-9}
		8.26 ± 0.01	

Note. – $F_{0.5-10}$ gives the unabsorbed 0.5–10 keV continuum flux. The line widths were unconstrained when left to vary and were therefore fixed to $\sigma_l = 10^{-4}$. Errors reflect 1σ uncertainties.

gaps near the inferred line energies. However, given the low significance and unclear physical interpretation, we consider it most likely that the 8.26 keV feature is spurious (see Section 3.3.3). Moreover, we point out that there are also several concerns about the physical interpretation of the $\simeq 7.64$ keV feature (see Section 4.1).

3.3.3 Photo-ionization modeling of the *Chandra* data

Assuming that the narrow lines in the *Chandra*/HEG data are real, we briefly explored what physical properties of the absorbing gas would be required to give rise to these features. To this end, we created a grid of self-consistent photoionization models with XSTAR

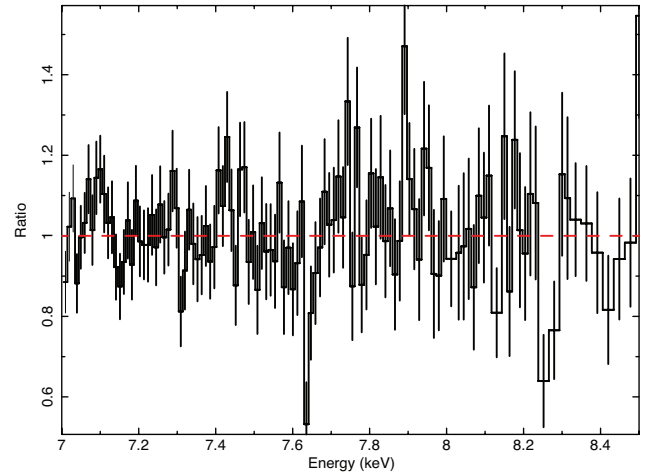


Figure 5. Data to model ratio in the *Chandra*/HEG data zoomed at the 7–8.5 keV range. Narrow absorption features are seen near $\simeq 7.6$ and 8.2 keV.

(Kallman & Bautista 2001). These were read into XSPEC as a multiplicative model to fit the HEG spectral data. The XSTAR modeling can be regarded as a consistency check to determine if it is possible to create the observed absorption lines with reasonable physical parameters, without producing any other obvious features that are not seen.

To create a grid for RXS J1804, we extrapolated our continuum fit to an energy range of 0.2–35 keV and supplied this to XSTAR as the source of ionizing flux with a bolometric luminosity of $L=5 \times 10^{37} \text{ erg s}^{-1}$ (inferred from extrapolating our continuum fit to 0.01–100 keV). We used a fiducial covering factor of $\Omega/4\pi=0.5$, which is typically a good assumption for disk winds in LMXBs (e.g., Miller et al. 2015). Furthermore, we assumed a number density of $n=10^{12} \text{ cm}^{-3}$, a turbulent velocity of 200 km s^{-1} , and Solar abundances as input for the grid calculations. The fit parameters for our XSTAR model are the matter density N , the ionization parameter ξ , and the blueshift v_{out} . Since these fits are non-unique and are only intended to be exploratory, we do not give errors on the fit parameters.

The most abundant elements seen in absorption in the X-ray spectra of LMXBs are Fe XXV (rest wavelength 6.70 keV) and Fe XXVI (rest wavelength 6.97 keV), which can be red/blue shifted in case of an in/outflow (e.g., Ponti et al. 2012; Díaz Trigo & Boirin 2016). We found that any model fitting the $\simeq 7.64$ keV line as blue-shifted Fe XXV predicts a strong Fe XXVI line at commensurate blue-shift ($\simeq 7.98$ keV), which is not seen. A higher density or lower ionization does not solve this issue, as that results in prominent absorption lines near 2.3 and 3 keV that are not seen either.

The 7.64 and 8.26 keV features can thus not arise from the same absorbing plasma, as the implied blueshifts would be different. Given this discrepancy and the low significance of the 8.26 keV feature ($\simeq 2\sigma$ after accounting for the number of trials), we consider it likely that this feature is spurious. If we assume that only the $\simeq 7.64$ keV line is real, its most likely interpretation is blue-shifted Fe XXVI and would thus suggest an outflow. We can then model this feature with $N \simeq 2 \times 10^{22} \text{ cm}^{-2}$ and $\log \xi \simeq 4.3$, which are plausible values for LMXBs. With these gas parameters no other absorption lines should be seen, consistent with our data. The implied outflow velocity is $v_{out} \simeq 0.086c \simeq 25\,800 \text{ km s}^{-1}$. We note that the gas density and ionization parameter obtained for this exploratory

fit should not be taken at face value. In particular, the geometry of the putative absorber in RXS J1804 is unclear (see Section 4.1) and the covering fraction is degenerate with the column density.

4 DISCUSSION

We report on *NuSTAR*, *Swift*, and *Chandra* observations obtained during a $\simeq 11$ -day window around the peak brightness of the 2015 outburst of the neutron star LMXB RXS J1804. The broad-band 0.7–35 keV *NuSTAR/Swift* spectral data can be described by a continuum model composed of a disk black body and thermal Comptonization. The source was in a soft spectral state during our observations and we measured a 0.5–10 keV luminosity of $L_{0.5-10} \simeq (2-3) \times 10^{37} (D/5.8 \text{ kpc})^2 \text{ erg s}^{-1}$. Assuming a bolometric correction factor of 2–3 (e.g., in 't Zand et al. 2007), this corresponds to $\simeq 10\%$ – 25% of the Eddington limit ($L_{\text{Edd}} = 3.8 \times 10^{38} \text{ erg s}^{-1}$; Kuulkers et al. 2003).

Superimposed on the continuum, we detect a broad Fe-K emission line that likely arises from hard X-rays reflecting off the accretion disk. Modeling this feature as relativistically blurred reflection allows us to constrain the accretion geometry in the soft state. We find a disk inclination of $i = 29^\circ$ – 35° (1σ confidence level), consistent with results obtained from reflection analysis in the hard state of the same RXS J1804 outburst ($i = 18^\circ$ – 29° at 90% confidence; Ludlam et al. 2016).

Our analysis suggests that the inner edge of the accretion disk extended inwards to $R_{\text{in}} \simeq 5$ – $7.5 R_g$ ($\simeq 11$ – 17 km). Bearing in mind the caveats stated in Section 3.2, we note that a similar inner disk radius is implied by the normalization of the disk black body component in our spectral fits ($R_{\text{in}} \simeq 9.5$ – 11 km). These values are consistent with the expected radius of a neutron star (e.g., Lattimer & Steiner 2014, for a recent overview), which suggests that the accretion disk may have been truncated by the stellar surface (and hence that the ISCO lies within the neutron star).

The inner disk may have also been truncated by the magnetic field of the neutron star, rather than its surface. We can thus use our measured inner disk radius to estimate an upper limit for the magnetic field strength of the neutron star. To this end we use equation (1) of Cackett et al. (2009a), which was adapted from the formulation of Ibragimov & Poutanen (2009). Extrapolating our *NuSTAR/Swift* spectral fit to 0.01–100 keV suggests a bolometric flux of $F_{\text{bol}} \simeq 1.2 \times 10^{-8} \text{ erg cm}^{-2} \text{ s}^{-1}$. We assume $D = 5.8 \text{ kpc}$, $M = 1.5 M_\odot$, $R = 10 \text{ km}$ and make similar assumptions regarding geometry and the accretion efficiency as in Cackett et al. (2009a); an anisotropy correction factor $f_{\text{ang}} = 1$, a geometry coefficient $k_A = 0.5$, and an accretion efficiency $\eta = 0.1$. The constraint that $R_{\text{in}} \lesssim 7.5 R_g$, then yields $B \lesssim 2 \times 10^8 \text{ G}$ for RXS J1804.

4.1 On the possible detection of a disk wind

We detect a narrow absorption line at $\simeq 7.64 \text{ keV}$ in our *Chandra*/HEG data that is $\simeq 4.8\sigma$ significant after accounting for the number of trials. Other narrow absorption features were seen in the *Chandra*/HEG data and two of the *Swift*/XRT soft-state observations at energies of $\simeq 7$ – 8 keV , but at lower significance ($\simeq 2$ – 4σ after accounting for trials). Blue-shifted, narrow absorption lines have been seen in several black hole and neutron star LMXBs during their soft states, and are interpreted as outflowing disk winds (e.g., Brandt & Schulz 2000; Lee et al. 2002; Ueda et al. 2004; Miller et al. 2006b, 2008, 2011, 2016; Díaz Trigo et al. 2007;

Neilsen & Lee 2009; Neilsen et al. 2011; King et al. 2012, 2015; Ponti et al. 2012; Degenaar et al. 2014a; Bozzo et al. 2016).

Since RXS J1804 was in a soft state during the observations analyzed in this work, it is plausible that a disk wind was present. Assuming that the 7.64 keV line in our *Chandra* data is both real and due to a disk wind, our photo-ionization modeling suggests that the most likely identification is blue-shifted Fe XXVI, which would imply an outflow velocity of $\simeq 0.086c \simeq 25\,800 \text{ km s}^{-1}$. However, we note that a solid identification is not trivial with just a single line. Moreover, there are several concerns about interpreting this feature as being due to a fast, outflowing disk wind.

Firstly, observational evidence suggests that disk winds are concentrated in the accretion disk plane (e.g., Miller et al. 2006a,b, 2015; King et al. 2012; Ponti et al. 2012; Degenaar et al. 2014b). Indeed, simulations of (thermally-driven) disk winds suggest that at near-polar angles, the low density and high ionization of the gas may prevent its detection (e.g., Sim et al. 2008; Higginbottom & Proga 2015). However, our spectral analysis suggests that RXS J1804 is seen at a relatively low inclination of $i \simeq 30^\circ$ (see also Ludlam et al. 2016). It is therefore not clear whether a disk wind, if present, would be observable. Nevertheless, a signature of a wind was recently reported for the neutron star LMXB GX 340+0, which has a similarly low inclination of $i \simeq 35^\circ$ (Miller et al. 2016). It was proposed that in this source the wind may be radiatively or magnetically driven (see e.g., Díaz Trigo & Boirin 2016, for a discussion on wind driving mechanisms). Indeed, simulations of magnetically-driven winds in LMXBs suggest that these may be observable at lower inclination angles (e.g., Chakravorty et al. 2016).

Secondly, the implied outflow velocity of $\simeq 25\,800 \text{ km s}^{-1}$ ($\simeq 0.086c$) would be extreme for an LMXB. Such fast outflows are not uncommon in supermassive black holes (e.g., Tombesi 2016, for a recent review), but wind velocities tend to be more modest in LMXBs. The highest velocities claimed for LMXBs so far are $\simeq 9\,000$ – $14\,000 \text{ km s}^{-1}$ ($\simeq 0.03$ – $0.04c$; King et al. 2012; Degenaar et al. 2014a; Miller et al. 2016), but more typical values are $\simeq 400$ – $3\,000 \text{ km s}^{-1}$ ($\simeq 0.001$ – $0.01c$; e.g., Díaz Trigo & Boirin 2016, for an overview). Wind velocities in LMXBs are thus commonly a factor > 10 lower than implied for RXS J1804, and even the most extreme cases so far have a factor > 3 lower outflow velocities than we find.

Although there is reason to be skeptical about the detection of the $\simeq 7.64 \text{ keV}$ line, we briefly speculate on its possible implication assuming that it is both real and that its interpretation as blue-shifted Fe XXVI is correct. Observations seem to suggest that winds and jets generally do not co-exist, and leave room for the possibility that winds and jets perhaps evolve into one another (e.g., Miller et al. 2006a; Neilsen & Lee 2009; King et al. 2012; Ponti et al. 2012; Díaz Trigo et al. 2013). If so, winds may accelerate and become denser away from the disk plane when moving toward lower luminosity. This could perhaps account for detecting a fast outflow from RXS J1804 in our *Chandra* observations, as it was accreting at a relatively low luminosity of $L_{0.5-10} \simeq 2 \times 10^{37} (D/5.8 \text{ kpc})^2 \text{ erg s}^{-1}$ at the time. Within this context it is interesting to note that RXS J1804 was detected at radio wavelengths on 2015 April 12, just two days before our *Chandra* observation, albeit with a much lower flux density than during the preceding hard spectral state (Gusinskaia et al., in preparation).

It is also possible that the neutron star magnetic field acts as a propeller and ejects material. MHD simulations of Romanova et al. (2009) reveal both a jet-like and a wind-like outflow for an active propeller. In these simulations the wind component is a thin con-

ical shell with a half-opening angle of $\simeq 30^\circ\text{--}40^\circ$ and a velocity up to $\simeq 0.1c$. Such an outflow may be compatible with our X-ray observations of RXS J1804 and the quasi-simultaneous weak radio detection. In particular, the putative X-ray absorption lines are very narrow and it would require a thin ejected shell to be internally consistent with the radial velocity implied by the blue-shift.

A propeller operates when the magnetospheric radius is larger than the co-rotation radius (i.e., the radius at which the Keplerian frequency of the disk is equal to the spin frequency of the neutron star). If the inner disk in RXS J1804 were to be truncated by the magnetosphere and this radius ($R_{\text{in}} \lesssim 17$ km) were to be larger than the co-rotation radius, then the neutron star would have to be spinning at $\lesssim 0.4$ ms. However, no neutron stars with sub-millisecond spin periods are known to date (e.g., Patruno et al. 2012).

In summary, there is an absorption feature significantly detected at $\simeq 7.64$ keV in our *Chandra*/HEG data that can plausibly be identified as blue-shifted Fe XXVI and arise from a disk wind. However, this would require that winds in neutron star LMXBs are observable at low inclination angles of $i \simeq 30^\circ$, and are able to reach an outflow velocity as high as $v_{\text{out}} \simeq 25\,800$ km s $^{-1}$.

4.2 On the size of the binary orbit

Baglio et al. (2016) reported that an optical spectrum obtained in late April, after RXS J1804 had transitioned to the soft X-ray spectral state, was featureless apart from a possible HeII emission line at 4686 Å. Based on the lack of H-emission lines, which are usually seen in the optical spectra of LMXBs, the authors proposed that the donor star must be H poor and thus that RXS J1804 is a candidate ultra-compact X-ray binary (UCXB). UCXBs are X-ray binaries in which the donor is an evolved star in a tight $P_{\text{orb}} \lesssim 90$ min orbit. Baglio et al. (2016) estimated the time-averaged mass-accretion rate of RXS J1804 based on *RXTE*/ASM and *MAXI* monitoring, and concluded that this is broadly consistent with the source having a He-rich donor in a $\simeq 40$ min orbit, based on a comparison with the disk instability model (Lasota (2008); see also the evolutionary tracks of van Haaften et al. (2012)).

We note that the lack of H-emission lines during single-epoch spectroscopy does not necessarily have to imply an UCXB nature. There are a few (black hole) LMXBs that did not show H-emission lines in their optical outburst spectra at some epochs, but have measured orbital periods of $P_{\text{orb}} \gtrsim 90$ min: e.g., Swift J1357.2–0933 (Torres et al. 2011), and Swift J1753.5–0127, (Jonker et al. 2008). Nevertheless, their orbits are relatively small: $P_{\text{orb}} = 2.8$ and 2.85 or 3.2 hr, respectively (Zurita et al. 2008; Corral-Santana et al. 2013; Neustroev et al. 2014). This may suggest a possible link between a short orbital period and the absence of H-emission lines. Indeed, there are several additional arguments that would support a relatively short orbital period for RXS J1804.

Firstly, the full-width half maximum (FWHM) of the tentative HeII 4686-Å line identified by Baglio et al. (2016) is quite low. From their figure 1, we estimate a FWHM of $\simeq 15$ Å and hence an equivalent resolved velocity of $\simeq 960$ km s $^{-1}$. If a similar FWHM- K_2 correlation as recently found by Casares (2015) would apply for He and during outburst, this would suggest a low velocity amplitude of the companion star of $K_2 = 0.233 \times \text{FWHM} \simeq 224$ km s $^{-1}$. For a short orbital period of 1–3 hr and a very small mass ratio (applicable for a short period system), the mass function then is $f \simeq 0.05\text{--}0.14 M_{\odot}$. For a 1.5 M_{\odot} neutron star, this implies a low inclination of $i \simeq 19^\circ\text{--}27^\circ$, which is remarkably similar to that obtained from modeling the Fe-K line in the X-ray spectra ($i \simeq 18^\circ\text{--}35^\circ$; this work and Ludlam et al. 2016). Such a low inclination

could account for the lack of orbital signatures in the optical data (Baglio et al. 2016), as ellipsoidal modulations would be small.

Secondly, the orbital period of LMXBs correlates with their absolute visual magnitude and X-ray luminosity (van Paradijs & McClintock (1994), see also Russell et al. (2006)). We measured an X-ray luminosity of $L_{0.7\text{--}35} \simeq 2 \times 10^{37}$ erg s $^{-1}$ on 2015 April 14, whereas Baglio et al. (2016) reported an apparent visual magnitude of $\simeq 17$ mag on 2015 April 24 (see their table 2). For $D = 5.8$ kpc, we can then roughly estimate an orbital period of $P_{\text{orb}} = 2.7$ hr using the empirical relation of van Paradijs & McClintock (1994).

The X-ray spectral shape may also provide clues about the size of the binary. Sidoli et al. (2001) analyzed the broad-band (0.1–100 keV) spectra of a sample of Galactic globular cluster LMXBs, fitting these with a disk black body and a Comptonizing component. These authors found that only in the (candidate) UCXBs, the obtained inner disk temperatures were similar to that of the seed photons of the Comptonized emission, and the obtained radii (several km) broadly consistent with that expected for the location of the inner disk. For the non-UCXBs, the inner disk temperatures were much higher ($\simeq 2\text{--}3$ keV), and their radii un-physically small ($\lesssim 1$ km). This seems to suggest that only in UCXBs, the region providing the seed photons of the Comptonized emission is small and consistent with the inner accretion disk (Sidoli et al. 2001).

The tentative classification scheme of Sidoli et al. (2001) gained credence through testing for an UCXB nature by alternative methods such as the relation of van Paradijs & McClintock (1994) discussed above, and the composition of the accreted matter inferred from thermonuclear X-ray bursts (see Verbunt & Lewin 2006). Its validity has also been strengthened by a number of additional sources (e.g., Gierliński & Poutanen 2005; Falanga et al. 2005; Fionchi et al. 2008). However, Engel et al. (2012) identified a 2.15-hr orbital period for XB 1832–330 in the Galactic globular cluster NGC 6652, which was originally put forward as an UCXB based on the spectral-shape classification (Parmar et al. 2001). It was therefore proposed by Stacey et al. (2012), that the Sidoli et al. (2001) scheme may not strictly apply to UCXBs (i.e., with $P_{\text{orb}} \lesssim 90$ min), but can still distinguish between short and long orbital period systems.

Against this background, we note that our fits of the 0.7–35 keV *Swift*/*NuSTAR* spectrum of RXS J1804 yield an inner disk temperature and seed photon temperature of the Comptonized component that are consistent within their 1σ errors; $kT_{\text{in}} = 1.15 \pm 0.02$ keV and $kT_s = 1.27 \pm 0.45$ keV, respectively. Furthermore, from the continuum spectral shape we obtain an inner disk radius of $\simeq 9.5\text{--}11$ km if we boldly apply a color-correction factor of 1.7 (see Section 3.2 for caveats), i.e., consistent with inner disk radius measured from the reflection component. The Sidoli et al. (2001) classification scheme would thus favor a small disk size, hence small orbital period, for RXS J1804.

Finally, the maximum luminosity that can be reached during outburst should scale with the orbital period of the binary (e.g., Lasota 2001), which is borne out by observations (e.g., Wu et al. 2010). For the estimated bolometric peak X-ray luminosity of RXS J1804 ($L_{\text{bol}} \simeq 5 \times 10^{37}$ erg s $^{-1}$), the empirical relation of Wu et al. (2010) yields an orbital period of $\simeq 1.4$ hr. Disk instability theory predicts an orbital period of $\simeq 2.4$ hr for an irradiated He disk (Lasota et al. 2008). A He-dominated disk would be consistent the lack of H-features and presence of HeII emission in the optical spectra (Baglio et al. 2016). We note that if RXS J1804 harbors an evolved companion, the detection of Fe-K reflection in both the soft and the hard X-ray spectral state might argue in

favor of a He donor rather than a C/O or O/Ne/Mg white dwarf donor, since a high C/O abundance could screen Fe and hence suppress the Fe-K line in C/O rich systems (Koliopanos et al. (2013), Koliopanos et al. (2014), but see Madej et al. (2014)).

In conclusion, the lack of H and the narrowness of the tentative He line in the optical spectrum, the X-ray and optical luminosity, the broad-band X-ray spectral shape, and the peak X-ray luminosity are all consistent with RXS J1804 being a neutron star LMXB with a relatively small orbit of $P_{\text{orb}} \lesssim 3$ hr.

ACKNOWLEDGEMENTS

We are grateful to Belinda Wilkes, Fiona Harrison, Neil Gehrels and the *Chandra*, *NuSTAR* and *Swift* teams for carrying out these DDT observations. The authors thank the anonymous referee for constructive comments. N.D. thanks Ciro Pinto, Matt Middleton and Anne Lohfink for useful discussions. N.D. is supported by an NWO/Vidi grant and an EU Marie Curie Intra-European fellowship under contract no. FP-PEOPLE-2013-IEF-627148. D.A. acknowledges support from the Royal Society. J.C.A.M.J. is supported by an Australian Research Council (ARC) Future Fellowship (FT140101082) and an ARC Discovery Grant (DP120102393). R.W. and A.P. are supported by an NWO/TOP grant, module 1, awarded to R.W. C.O.H. is supported by an NSERC Discovery Grant. A.T.D. is supported by an NWO/Veni grant. J.W.T.H. is supported by NWO/Vidi and ERC/starting (337062) grants.

REFERENCES

- Arnaud K., 1996, in G. Jacoby, J. Barnes, eds, *Astronomical Data Analysis Software and Systems V*. Astronomical Society of the Pacific Conference Series, Vol. 101, p. 17
- Baglio M. C., D’Avanzo P., Campana S., Goldoni P., Masetti N., Muñoz-Darias T., Patiño-Álvarez V., Chavushyan V., 2016, *A&A*, 587, A102
- Barret D., Olive J. F., 2002, *ApJ*, 576, 391
- Barret D., Olive J., Boirin L., Done C., Skinner G., Grindlay J., 2000, *ApJ*, 533, 329
- Begelman M., McKee C., 1983, *ApJ*, 271, 89
- Bhattacharyya S., Strohmayer T., 2007, *ApJL*, 664, L103
- Bozzo E. et al., 2016, *A&A*, 589, A42
- Braje T. M., Romani R. W., Rauch K. P., 2000, *ApJ*, 531, 447
- Brandt W., Schulz N., 2000, *ApJL*, 544, L123
- Cackett E., Altamirano D., Patruno A., Miller J., Reynolds M., Linares M., Wijnands R., 2009a, *ApJL*, 694, L21
- Cackett E. et al., 2010, *ApJ*, 720, 205
- Cackett E. M. et al., 2009b, *ApJ*, 690, 1847
- Canizares C. R. et al., 2000, *ApJL*, 539, L41
- Casares J., 2015, *ApJ*, 808, 80
- Chakravorty S. et al., 2016, *A&A*, 589, A119
- Chenevez J. et al., 2012, *ATel*, 4050
- Chiang C. Y. et al., 2016, *ApJ*, 821, 105
- Corral-Santana J., Casares J., Muñoz-Darias T., Rodríguez-Gil P., Shahbaz T., Torres M., Zurita C., Tyndall A., 2013, *Science*, 339, 1048
- D’Ai A., Iaria R., Di Salvo T., Matt G., Robba N., 2009, *ApJL*, 693, L1
- Degenaar N., Miller J. M., Harrison F. A., Kennea J. A., Kouveliotou C., Younes G., 2014a, *ApJL*, 796, L9
- Degenaar N., Miller J. M., Chakrabarty D., Harrison F. A., Kara E., Fabian A. C., 2015a, *MNRAS*, 451, L85
- Degenaar N. et al., 2014b, *ApJ*, 784, 122
- Degenaar N. et al., 2015b, *ATel*, 7352
- Deller A. et al., 2015, *ATel*, 7255
- Di Salvo T., Iaria R., Burderi L., Robba N. R., 2000, *ApJ*, 542, 1034
- Di Salvo T. et al., 2015, *MNRAS*, 449, 2794
- Díaz Trigo M., Boirin L., 2016, *Astronomische Nachrichten*, 337, 368
- Díaz Trigo M., Parmar A., Miller J., Kuulkers E., Caballero-García M., 2007, *A&A*, 462, 657
- Díaz Trigo M., Miller-Jones J. C. A., Migliari S., Broderick J. W., Tzioumis T., 2013, *Nature*, 504, 260
- Engel M. C., Heinke C. O., Sivakoff G. R., Elshamouty K. G., Edmonds P. D., 2012, *ApJ*, 747, 119
- Falanga M. et al., 2005, *A&A*, 436, 647
- Fiocchi M., Bazzano A., Ubertini P., De Cesare G., 2008, *A&A*, 477, 239
- Galloway D., Muno M., Hartman J., Psaltis D., Chakrabarty D., 2008, *ApJS*, 179, 360
- Gehrels N. et al., 2004, *ApJ*, 611, 1005
- George I. M., Fabian A. C., 1991, *MNRAS*, 249, 352
- Gierliński M., Poutanen J., 2005, *MNRAS*, 359, 1261
- Gierliński M., Zdziarski A. A., Poutanen J., Coppi P. S., Ebisawa K., Johnson W. N., 1999, *MNRAS*, 309, 496
- Harrison F. A. et al., 2013, *ApJ*, 770, 103
- Higginbottom N., Proga D., 2015, *ApJ*, 807, 107
- Homan J., Belloni T., 2005, *Ap&SS*, 300, 107
- Ibragimov A., Poutanen J., 2009, *MNRAS*, 400, 492
- in ’t Zand J., Jonker P., Markwardt C., 2007, *A&A*, 465, 953
- Jonker P. G., Torres M. A. P., Steeghs D., 2008, in R.M. Bandyopadhyay, S. Wachter, D. Gelino, C.R. Gelino, eds, *A Population Explosion: The Nature & Evolution of X-ray Binaries in Diverse Environments*. American Institute of Physics Conference Series, Vol. 1010, pp. 109–116
- Kallman T., Bautista M., 2001, *ApJS*, 133, 221
- Kaur R., Heinke C., 2012, *ATel*, 4085
- King A. et al., 2012, *ApJL*, 746, L20
- King A. L., Miller J. M., Raymond J., Reynolds M. T., Morningstar W., 2015, *ApJL*, 813, L37
- King A. L. et al., 2016, *ApJL*, 819, L29
- Koliopanos F., Gilfanov M., Bildsten L., 2013, *MNRAS*, 432, 1264
- Koliopanos F., Gilfanov M., Bildsten L., Trigo M. D., 2014, *MNRAS*, 442, 2817
- Krimm H. et al., 2013, *ApJS*, 209, 14
- Krimm H. A., Kennea J. A., Siegel M. H., Sbarufatti B., 2015a, *ATel*, 7039
- Krimm H. A. et al., 2015b, *ATel*, 6997
- Kubota A., Makishima K., Ebisawa K., 2001, *ApJL*, 560, L147
- Kuulkers E., den Hartog P., in ’t Zand J., Verbunt F., Harris W., Cocchi M., 2003, *A&A*, 399, 663
- Lasota J. P., 2001, *NewAR*, 45, 449
- Lasota J. P., 2008, *NewAR*, 51, 752
- Lasota J. P., Dubus G., Kruk K., 2008, *A&A*, 486, 523
- Lattimer J. M., Steiner A. W., 2014, *ApJ*, 784, 123
- Lee J. C., Reynolds C. S., Remillard R., Schulz N. S., Blackman E. G., Fabian A. C., 2002, *ApJ*, 567, 1102
- Lin D., Remillard R., Homan J., 2007, *ApJ*, 667, 1073
- Ludlam R. M. et al., 2016, *ApJ*, 824, 37

- Madej O. K., García J., Jonker P. G., Parker M. L., Ross R., Fabian A. C., Chenevez J., 2014, *MNRAS*, 442, 1157
- Matsuoka et al. M., 2009, *PASJ*, 61, 999
- Matt G., Perola G. C., Piro L., 1991, *A&A*, 247, 25
- Merloni A., Fabian A. C., Ross R. R., 2000, *MNRAS*, 313, 193
- Miller J., Raymond J., Reynolds C., Fabian A., Kallman T., Homan J., 2008, *ApJ*, 680, 1359
- Miller J., Maitra D., Cackett E., Bhattacharyya S., Strohmayer T., 2011, *ApJL*, 731, L7
- Miller J. et al., 2006a, *ApJ*, 646, 394
- Miller J., Raymond J., Fabian A., Steeghs D., Homan J., Reynolds C., van der Klis M., Wijnands R., 2006b, *Nature*, 441, 953
- Miller J. et al., 2012, *ApJL*, 759, L6
- Miller J. et al., 2013, *ApJL*, 779, L2
- Miller J. M., Raymond J., Cackett E., Grinberg V., Nowak M., 2016, *ApJL*, 822, L18
- Miller J. M., Fabian A. C., Kaastra J., Kallman T., King A. L., Proga D., Raymond J., Reynolds C. S., 2015, *ApJ*, 814, 87
- Miller M. C., Lamb F. K., Cook G. B., 1998, *ApJ*, 509, 793
- Negoro H. et al., 2015, *ATel*, 7008
- Neilsen J., Lee J., 2009, *Nature*, 458, 481
- Neilsen J., Remillard R. A., Lee J. C., 2011, *ApJ*, 737, 69
- Neustroev V. V., Veledina A., Poutanen J., Zharikov S. V., Tsygankov S. S., Sjoberg G., Kajava J. J. E., 2014, *MNRAS*, 445, 2424
- Ng C., Díaz Trigo M., Cadolle Bel M., Migliari S., 2010, *A&A*, 522, A96
- Papitto A., Di Salvo T., D’Ài A., Iaria R., Burderi L., Riggio A., Menna M., Robba N., 2009, *A&A*, 493, L39
- Parmar A. N., Oosterbroek T., Sidoli L., Stella L., Frontera F., 2001, *A&A*, 380, 490
- Patruno A., Haskell B., D’Angelo C., 2012, *ApJ*, 746, 9
- Pintore F. et al., 2016, *MNRAS*, 457, 2988
- Piraino S., Santangelo A., di Salvo T., Kaaret P., Horns D., Iaria R., Burderi L., 2007, *A&A*, 471, L17
- Ponti G., Fender R., Begelman M., Dunn R., Neilsen J., Coriat M., 2012, *MNRAS*, 422, L11
- Remillard R., McClintock J., 2006, *ARAA*, 44, 49
- Reynolds M., Miller J., 2013, *ApJ*, 769, 16
- Romano P. et al., 2006, *A&A*, 456, 917
- Romanova M. M., Ustyugova G. V., Koldoba A. V., Lovelace R. V. E., 2009, *MNRAS*, 399, 1802
- Ross R., Fabian A., 2005, *MNRAS*, 358, 211
- Russell D., Fender R., Hynes R., Brocksopp C., Homan J., Jonker P., Buxton M., 2006, *MNRAS*, 371, 1334
- Shields G. A., McKee C. F., Lin D. N. C., Begelman M. C., 1986, *ApJ*, 306, 90
- Sidoli L., Parmar A. N., Oosterbroek T., Stella L., Verbunt F., Masetti N., Dal Fiume D., 2001, *A&A*, 368, 451
- Sim S. A., Long K. S., Miller L., Turner T. J., 2008, *MNRAS*, 388, 611
- Stacey W. S., Heinke C. O., Cohn H. N., Lugger P. M., Bahramian A., 2012, *ApJ*, 751, 62
- Tombesi F., 2016, *Astronomische Nachrichten*, 337, 410
- Torres M., Steeghs D., Jonker P., Rauch M., 2011, *ATel*, 3143
- Ueda Y., Murakami H., Yamaoka K., Dotani T., Ebisawa K., 2004, *ApJ*, 609, 325
- van Haften L., Nelemans G., Voss R., Wood M., Kuijpers J., 2012, *A&A*, 537, A104
- van Paradijs J., McClintock J., 1994, *A&A*, 290, 133
- Verbunt F., Lewin W., 2006, *Globular cluster X-ray sources*. pp. 341–379
- Verner D., Ferland G., Korista K., Yakovlev D., 1996, *ApJ*, 465, 487
- Voges W. et al., 1999, *A&A*, 349, 389
- Weisskopf M. C., Tananbaum H. D., Van Speybroeck L. P., O’Dell S. L., 2000, in J.E. Truemper, B. Aschenbach, eds, *X-Ray Optics, Instruments, and Missions III*. Proc. SPIE, Vol. 4012, pp. 2–16
- Wilms J., Allen A., McCray R., 2000, *ApJ*, 542, 914
- Wu Y. X., Yu W., Li T. P., Maccarone T. J., Li X. D., 2010, *ApJ*, 718, 620
- Zdziarski A. A., Johnson W. N., Magdziarz P., 1996, *MNRAS*, 283, 193
- Zurita C., Durant M., Torres M., Shahbaz T., Casares J., Steeghs D., 2008, *ApJ*, 681, 1458
- Życki P. T., Done C., Smith D. A., 1999, *MNRAS*, 309, 561